

Cite this: *Catal. Sci. Technol.*, 2019,
9, 1208

Electrochemical synthesis of ammonia from N₂ and H₂O using a typical non-noble metal carbon-based catalyst under ambient conditions†

Linchuan Cong,^a Zhuochen Yu,^a Fangbing Liu^a and Weimin Huang *^{ab}

Ammonia is an important precursor of fertilizers and nitrogen compounds, and it is also a potential energy storage medium and alternative fuel for vehicles. The main ammonia production process is the Haber-Bosch process, which is energy- and capital-intensive. Therefore, it is crucial to find an alternative method for the synthesis of ammonia. In this paper, we reported a new non-noble metal N-doped nanocarbon/Fe₃C nanoparticle catalyst (NCF) for the electrochemical synthesis of ammonia, yielding an NH₃ production rate of 15.804 μg h⁻¹ mg_{cat}⁻¹ and Faradic efficiency (FE) as high as 2.72% at -0.4 V vs. RHE at room temperature and ambient pressure in 0.1 M KOH electrolyte. We believe that this work will provide a new opportunity to design a new non-noble metal catalyst for the nitrogen reduction reaction (NRR) and also open a new route to solve the global energy and ecological crisis.

Received 9th November 2018,
Accepted 26th January 2019

DOI: 10.1039/c8cy02316f

rsc.li/catalysis

1. Introduction

Ammonia (NH₃) is one of the chemicals with the highest production efficiency, and the total global NH₃ production has been more than 146 million tons since the 21st century.¹ Ammonia is an important fertilizer and nitrogen compound precursor. About 80% of the produced NH₃ is used as a fertilizer precursor to provide sufficient food for the growing world population.² It is also a potential energy storage medium and alternative fuel for vehicles because of its high energy density and lack of carbon dioxide emissions.³⁻⁷ The main ammonia production process is the Haber-Bosch process, invented in 1904, which requires high temperatures (350–500 °C) and high pressures (150–300 bar) in addition to highly efficient catalysts; this process is energy- and capital-intensive.⁸⁻¹¹ In recent years, reportedly, the production of ammonia consumed 2% of the global energy and was responsible for 0.5% of the carbon dioxide emissions.^{12,13} Therefore, a more environmental-friendly alternative synthesis process is needed, which will help produce NH₃ in a sustainable and ecological way in the future.

Due to the stability and chemical inertia of nitrogen, the N≡N (225 kcal mol⁻¹) bond in dinitrogen is one of the strongest chemical bonds; however, fixing nitrogen at an ambient

temperature and pressure is still a huge challenge.¹⁴ Many new processes are being developed in search of more efficient and economical processes and in view of the potential for increase in ammonia production. Recently, studies have shown that N₂ and H₂O can produce ammonia through electrochemical methods.¹⁵⁻²¹ Compared with the Haber-Bosch process, the electrochemical synthesis of NH₃ is a promising method, which can reduce energy consumption and avoid direct carbon emissions. However, since the theoretical potentials of the hydrogen evolution reaction (HER) and the nitrogen reduction reaction (NRR, 0.057 V vs. SHE) are very close, H₂ is the dominant product; because the reaction kinetics of the former is much faster, the competing HER significantly reduces the Faradaic efficiency (FE) of NRR.

In a typical proton conductive electrolyte cell, the nitrogen reduction reaction occurs at the cathode, and hydrogen gas is converted to H⁺ at the anode. The resulting proton H⁺ diffuses into the cathode, where it combines with the dissociated N to form NH₃. Tao *et al.* synthesized ammonia from hydrogen and nitrogen based on an SDC-ternary carbonate composite electrolyte, and the formation rate of ammonia was 5.39 × 10⁻⁹ mol s⁻¹ cm⁻² at 450 °C.²² The reaction required a high temperature and harsh conditions; in addition, hydrogen gas was used as the proton source for the production of ammonia. In the process of the electrochemical synthesis of ammonia, the transport and storage of hydrogen gas are also challenging, and there are certain safety risks. To avoid the use of hydrogen, Hideo Hosono *et al.*²³ reported an air- and water-stable electride Y₅Si₃ that used water as a proton source to synthesize ammonia after combination with nitrogen. The ammonia synthesis rate using Ru-loaded (7.8

^a College of Chemistry, Jilin University, Changchun 130012, China.

E-mail: huangwm@jlu.edu.cn

^b Key Laboratory of Physics and Technology for Advanced Batteries of Ministry of Education, Jilin University, Changchun 130012, China

† Electronic supplementary information (ESI) available. See DOI: 10.1039/c8cy02316f

wt%) Y_5Si_3 was as high as $1.9 \text{ mmol g}^{-1} \text{ h}^{-1}$ under 0.1 MPa and at $400 \text{ }^\circ\text{C}$ with activation energy of $\sim 50 \text{ kJ mol}^{-1}$. The reaction conditions were still harsh and required large energy consumption. Recently, Egill Skulason *et al.*²⁴ predicted that transition metal nitrides may play a role in NRR through the calculation of density functional theory (DFT), which proved the possibility of water and nitrogen electrochemical synthesis of ammonia in ambient conditions. Then, Yan *et al.*²⁵ used tetrahedral gold nanorods as a heterogeneous electrocatalyst to promote the N_2 reduction reaction at room temperature and atmospheric pressure, which showed electrocatalytic NRR with a high production yield (NH_3 : $1.648 \mu\text{g h}^{-1} \text{ cm}^{-2}$) and low activation energy ($\approx 13.704 \text{ kJ mol}^{-1}$) at -0.2 V vs. RHE .

Compared to noble metal catalysts, carbon-based catalysts are more abundant, cheap and readily available while mitigating the competing HER. Besides, doping with transition metals such as Fe, Co or Ni can improve the catalytic activity, and it has been recently found that N-doped carbons can facilitate the dissociation of N_2 and further suppress the activity for HER.^{26–29} Thus, we controlled the synthesis of new one-dimensional N-doped carbon nanotube/ Fe_3C nanoparticle hybrid (NCF) electrocatalysts, which were directly prepared by annealing a mixture of PEG–PPG–PEG Pluronic® P123, melamine, and $\text{Fe}(\text{NO}_3)_3$ at $800 \text{ }^\circ\text{C}$ in N_2 . The N-doped carbon nanotube/ Fe_3C nanoparticle hybrid electrocatalysts showed high NRR activity, yielding an NH_3 production rate of $15.804 \mu\text{g h}^{-1} \text{ mg}_{\text{cat.}}^{-1}$ and Faradic efficiency (FE) as high as 2.72% at -0.4 V vs. RHE at room temperature and ambient pressure in 0.1 M KOH electrolyte.

2. Experimental

2.1 Chemicals and materials

Melamine (the East China Chemical Reagent Company, $\text{C}_3\text{H}_6\text{N}_6$, Tianjin, China), iron nitrate (Beijing Chemical Reagent Company, $\text{Fe}(\text{NO}_3)_3$, Beijing, China), PEG–PPG–PEG Pluronic® P123 (Mw = 5800, Sigma-Aldrich), Nafion (5.0 wt%, Dupont), Nafion 117 membrane (Dupont), hydrochloric acid (Beijing Chemical Works, HCl, 35.0–38.0%), sulfuric acid (Beijing Chemical Works, H_2SO_4 , 98%), potassium chloride (Beijing Chemical Works, KCl, analytical reagent), ethyl alcohol (Beijing Chemical Works, $\text{C}_2\text{H}_5\text{OH}$, $\geq 99.8\%$), ammonium chloride (Beijing Chemical Works, NH_4Cl , analytical reagent), salicylic acid (Beijing Chemical Works, $\text{C}_7\text{H}_6\text{O}_3$, 99.5%), sodium citrate dehydrate (Beijing Chemical Works, $\text{C}_6\text{H}_5\text{Na}_3\text{O}_7 \cdot 2\text{H}_2\text{O}$, $\geq 99.0\%$), sodium hydroxide (Beijing Chemical Works, NaOH, 96%), potassium hydroxide (Beijing Chemical Works, KOH, 96%), sodium nitroferrocyanide dihydrate (Aladdin, $\text{C}_5\text{FeN}_6\text{Na}_2\text{O} \cdot 2\text{H}_2\text{O}$, 99%), sodium hypochlorite solution (Beijing Chemical Reagent Company, NaClO, available chlorine 4.0%), isopropyl alcohol (Beijing Chemical Works, $\text{C}_3\text{H}_8\text{O}$), nickel foam ($1 \times 1 \text{ cm}$), N_2 gas (99.99%), and Ar gas (99.99%) were employed. All chemical reagents were used as received without further purification. All aqueous solutions were prepared with ultrapure water (resistivity of $18.25 \Omega \text{ cm}$).

2.2 Physical characterization

In order to obtain morphology information of the obtained composites, transmission electron microscopy (TEM), energy-dispersive X-ray (EDX) spectroscopy, and elemental mapping were performed on an FEI Tecnai G20/JEM2010 microscope (accelerating voltage = 200 kV). X-ray photoelectron spectra (XPS) were recorded on an ESCALAB250 spectrometer (Thermo Electron Corporation) with an excitation source of Mg $\text{K}\alpha$ radiation to carry out surface composition and chemical state analyses of the products. X-ray diffraction (XRD) patterns were obtained using a D/max diffractometer (Rigaku, Japan) with a Cu $\text{K}\alpha$ radiation source ($\lambda = 1.541874 \text{ \AA}$) operating at 50.0 kV and 200.0 mA, and the diffraction data were recorded in the 2θ range of $20\text{--}80^\circ$ with a scan rate of 4 degrees per minute. Raman spectra were measured with a Renishaw 2000 model confocal microscopy Raman spectrometer with a CCD detector and a holographic notch filter (Renishaw Ltd., Gloucestershire, UK). The absorbance data were measured on a Beijing Purkinje General TU-1900 ultraviolet-visible (UV-vis) spectrophotometer. Gas adsorption-desorption (77 K) analyses were conducted using N_2 as the adsorbent on 3H-2000 PM2 (BeiShiDe Instrument, PR China). The specific surface area (SSA) was calculated *via* applying the Brunauer–Emmett–Teller (BET) model.

2.3 Cathode preparation

One g P123, 1.5 g melamine and 0.4 g iron nitrate were dissolved in 40 mL ultrapure water; the mixture was stirred for 2 h and further sonicated for 5 h. Then, the solvent was slowly evaporated at $80 \text{ }^\circ\text{C}$. The remaining powder was heated at a rate of $2 \text{ }^\circ\text{C min}^{-1}$ to get an N-doped carbon nanotube/ Fe_3C nanoparticle hybrid (NCF) in a tube furnace and was heated for 2 h, 2 h and 1 h at $200 \text{ }^\circ\text{C}$, $400 \text{ }^\circ\text{C}$ and $800 \text{ }^\circ\text{C}$, respectively, in an N_2 atmosphere.³⁰ Eight mg NCF and 50 μL Nafion solution (5 wt%) were dispersed in 500 μL isopropyl alcohol and 500 μL ultrapure water by sonicating for 1 h to form a homogeneous catalyst ink. Then, 50 μL of the dispersion was loaded onto a nickel foam ($1 \times 1 \text{ cm}$) electrode (NCF-X@Ni) and dried in an N_2 atmosphere at room temperature. For comparison, the N-doped carbon (NC@Ni) loaded, the Fe-doped carbon (CF@Ni) loaded and the non-loaded foam nickel (Ni) electrodes were also prepared.

2.4 Electrochemical measurements

The experiments were carried out in an H-type electrochemical cell at room temperature, which was separated by a Nafion 117 membrane. A schematic diagram of the experimental device is shown in Fig. S1.† It was found that all the ammonia was collected by the solution in the cathodic chamber and no ammonia was measured in the absorber. Thus, only the solution in the cathodic chamber after electrochemical catalysis was detected in the remaining experiments. Before the NRR test, the Nafion membrane was pretreated by heating in 5% H_2O_2 aqueous solution at $80 \text{ }^\circ\text{C}$ for

1 h, 5% H₂SO₄ aqueous solution at 80 °C for 1 h and ultrapure water at 80 °C for another 1 h. The electrochemical experiments were carried out with an advanced electrochemical system (PARSTAT 2273) using a three-electrode system. A prepared Ni foam electrode, Pt foil and Hg/HgO electrode (1 M KOH electrolyte) were used as the working electrode, counter electrode and reference electrode, respectively. All the measured potential values were calibrated by using the following equation: E vs. RHE = E vs. Hg/HgO + 0.095 + 0.059 pH. For the linear sweep voltammetry (LSV) measurements, the scan rate was set to 10 mV s⁻¹. For NRR, potentiostatic tests were conducted in an N₂ saturated 0.1 M KOH solution (70 mL) (the KOH electrolyte was purged with N₂ for 30 min before the measurement) at -0.2 V, 0.3 V, 0.4 V, 0.5 V, and 0.6 V. Pure N₂ (possible ammonia was removed using sulfuric acid) was continuously fed to the whole cathode. In addition, the effect of different N₂ flow rates on NRR was also considered. For comparison, potentiostatic tests were also carried out in an Ar saturated 0.1 M KOH solution at different potentials in this work.

2.5 Determination of ammonia

The indophenol blue method and spectrophotometric analysis were used to determine the NH₃ concentration of the electrolytes.^{31–33} The UV-vis diffuse reflectance spectra (UV-vis DRS) of the collected electrolytes were recorded at wavelengths from 300 to 800 nm, and the concentration of indophenol blue was determined using the absorbance at a wavelength of 690 nm. The concentration (μg mL⁻¹) of ammonia was calculated from a calibration curve prepared by using standard ammonium chloride with a series of concentrations. The ammonia production rates (r) were calculated by using eqn (1):

$$r_{[\text{NH}_3]} = ([\text{NH}_3] \times V)/(t \times A) \quad (1)$$

Here, [NH₃] is the concentration (μg mL⁻¹) of ammonia, V is the volume (mL) of electrolyte, t is the reaction time (h), and A is the surface area (cm²) of the working electrode. The Faraday efficiency (FE) for NRR was defined as the amount of charge used for the synthesis of ammonia divided by the total amount of charge passing through the electrode during the electrolysis process. Assuming three electrons are consumed to produce one NH₃ molecule, FE could be calculated using eqn (2):

$$\text{FE} = 3F \times [\text{NH}_3] \times 10^{-6} \times V/(17 \times Q) \quad (2)$$

Here, F is the Faraday constant, [NH₃] is the concentration (μg mL⁻¹) of ammonia, V is the volume (mL) of electrolyte and Q is the total charge.

3. Results and discussion

The precursors of NCF are melamine, Pluronic P123 and iron nitrate. P123 is a triblock polymer that has an ideal rod struc-

ture, while melamine is an N source. It was hoped that doping with iron will further increase the rate of NRR. These mixtures could be carbonized directly and formed an iron-containing nitrogen-doped carbon nanostructure by one-step thermal activation. As shown in Fig. 1a and b (and Fig. S2†), tubular carbon is seen in the transmission electron microscopy (TEM) image, and iron-based nanoparticles can be observed either at the inside or tip of the carbon nanotube. This structure exhibited a higher surface area, which helped create more exposed active sites per unit mass of the catalysts. We analyzed the element distribution of NCF through high-angle annular dark-field scanning transmission electron microscopy and its mapping images, as shown in Fig. 1c–g. C and N were uniformly distributed throughout the region, while iron was concentrated on the carbon nanoparticles. It is possible that iron and carbon bonded together to form iron carbonization. Then, the crystal structure of NCF was investigated by typical X-ray diffraction (XRD), as shown in Fig. 2a. A typical strong peak was observed at about 26°, corresponding to the (002) face of graphite carbon, which is a structural feature of carbon nanotubes. The corresponding diffraction peaks were also seen at 37.8, 45.0, 49.2 and 54.5°, which were in agreement with those of Fe₃C (JCPDS file no. 892867). All the characterizations proved the formation of NCF and revealed its morphology and structure.

In order to further understand the homogeneous distribution of each element, energy-dispersive X-ray (EDX) spectroscopy mapping was conducted for NCF, as shown in Fig. S3.† C content of 85.34 wt%, N content of 6.17 wt% and Fe content of 6.69 wt% were determined by elemental analysis (Table S1†). The iron content was further determined by thermogravimetric analysis (TGA). As shown in Fig. S4,† the amount of Fe in NCF is determined to be 6.83 wt%, which is

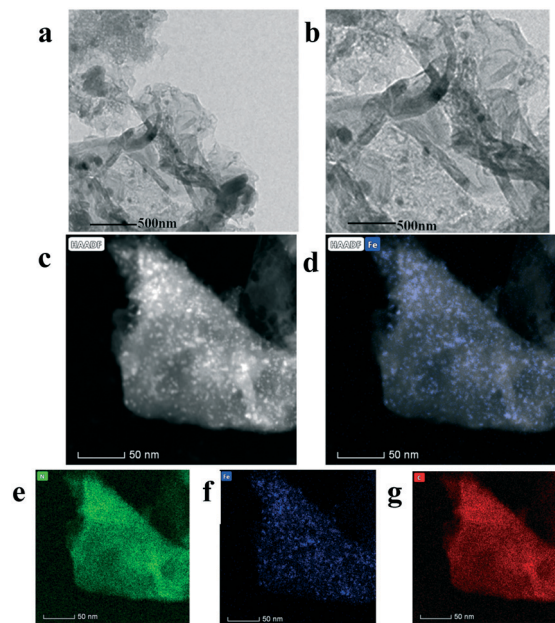


Fig. 1 (a and b) TEM images, (c) HAADF-STEM and (d–g) its mapping images of the resultant NCF.

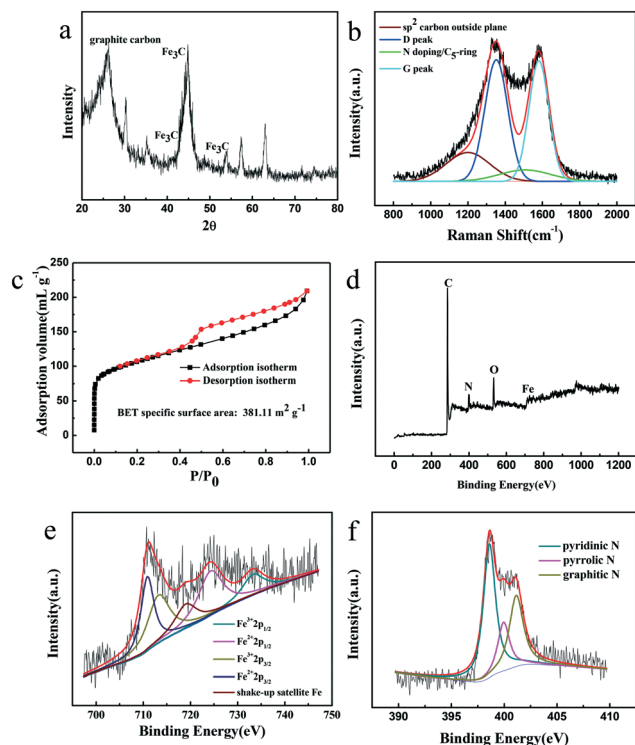


Fig. 2 (a) XRD pattern, (b) Raman spectrum, (c) nitrogen adsorption-desorption isotherm, (d) XPS survey spectrum, (e) Fe 2p XPS and (f) N 1s XPS high-resolution spectra for the resultant NCF.

consistent with the result of EDS. Generally, Fe doping can improve the performance of catalysts for electrochemical synthesis of ammonia. In order to understand the carbon structure in NCF and its effect on the NRR activity, Raman

spectroscopy was performed. As shown in Fig. 2b, the Raman spectra of the catalyst can be fitted into four types of carbon. The two most clear characteristic carbon resonances were found at 1600 cm^{-1} (G band) and 1350 cm^{-1} (D band), corresponding to the plane motion of sp^2 hybrid carbon atoms in the ideal carbon plane and the plane motion of edge carbon atoms.^{34,35} The ratio of these two peaks can be used as an indicator of the degree of graphitization in carbon. According to the graph and calculation, the I_D/I_G value is 1.02, indicating that NCF is highly graphitized, which is favourable for improving the conductivity of materials and further improving the catalytic efficiency of NRR. In addition, there are two broad peaks at 1200 cm^{-1} and 1510 cm^{-1} in the Raman spectra, which are correspondingly associated with the carbon atoms outside a perfectly planar sp^2 carbon network and integrated five-member rings or heteroatoms in carbon layers.³⁶ The specific surface area of a material is closely related to the number of active sites. Therefore, nitrogen adsorption-desorption experiments were conducted (Fig. 2c). The nitrogen adsorption-desorption isotherm was of type IV with distinct hysteresis loops, suggesting the co-existence of micro/mesopores in NCF. NCF exhibited larger BJH average pore diameter of 4.25 nm (Fig. S5†) and moderate total pore volume of 0.3238 mL g^{-1} . These hierarchical pores are favorable for the adsorption and transport of N_2 for further activation. The BET specific surface area of NCF was about $381.11\text{ m}^2\text{ g}^{-1}$. The larger specific surface area significantly increased the attachment sites of Fe_3C nanoparticles and enhanced the electrocatalytic activity of NCF. All these promoted the rate of electrochemical synthesis of ammonia. The catalytic activity of carbon-based materials can be further optimized by controlling the structure and specific surface area of carbon-based materials.

X-ray photoelectron spectroscopy (XPS) analysis (Fig. 2d) revealed that NCF mainly comprised C, N, Fe and O, confirming that N and Fe have been successfully doped into the carbon composite. The contents of Fe and N were 4.56% and 5.83%, respectively, which strongly indicated that Fe_3C has the chance to participate in surface catalysis. A high-resolution N 1s XPS spectrum (Fig. 2f) of NCF can be fitted into three types of N at 398.6, 400.2, and 401.1 eV, corresponding to pyridinic, pyrrolic, and graphitic nitrogen atoms. Pyridinic nitrogen atoms and graphitic nitrogen atoms were situated on the edge and interior of the carbon planes, respectively, and pyrrolic nitrogen atoms were present in a five-side carbon ring. Recently, some reports³⁷ have shown that a large proportion of pyridinic nitrogen can reduce the activation energy of nitrogen reduction and promote the electrochemical synthesis of ammonia. The higher content of pyridinic nitrogen in NCF was consistent with the higher NRR catalytic activity. In addition, the catalytic activity of NCF could be further optimized by regulating the species of nitrogen atoms. The high-resolution spectrum of Fe 2p in Fig. 2e shows that the Fe 2p signal can be deconvoluted into two pairs of peaks for Fe^{3+} (713.1 and 731.5 eV) and Fe^{2+} (710.8 and 724.3 eV). A signal at 707 eV was not observed, which indicated the absence of metallic iron, suggesting that the main

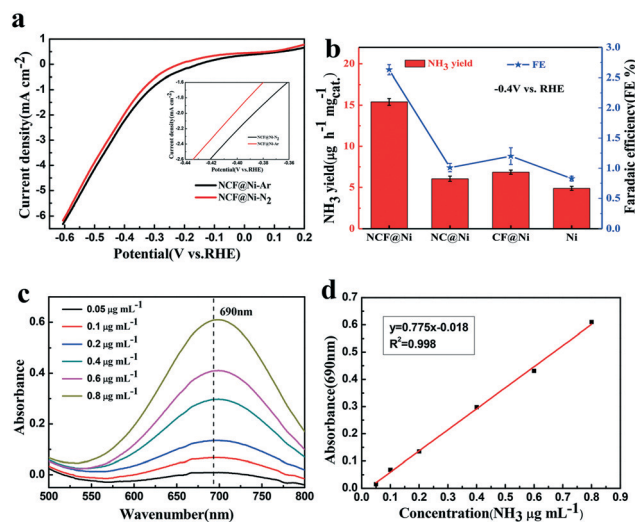


Fig. 3 (a) Linear sweep voltammograms in N_2 -saturated and Ar-saturated electrolyte using NCF catalysts. The curves of different electrodes were recorded in an aqueous solution of 0.1 M KOH under ambient conditions. The inset is the enlarged view from -0.44 to -0.36 V. (b) Yield rate of NH_3 with different catalysts at -0.4 V vs. RHE . (c) UV-vis curves of indophenol tests with NH_4^+ ions. (d) Calibration curve used for the estimation of NH_3 .

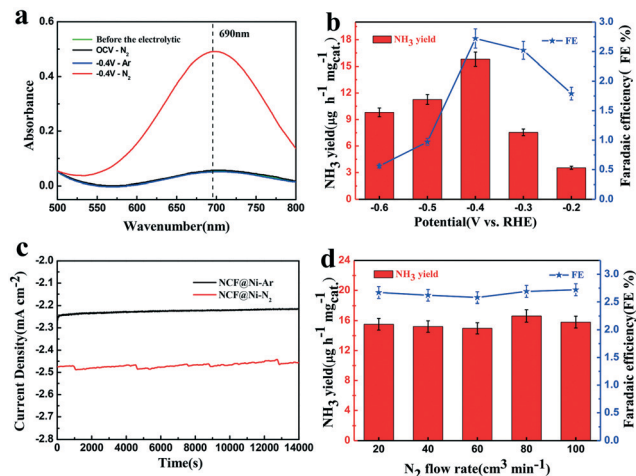


Fig. 4 (a) UV-vis curves of indophenol tests under different conditions. (b) Yield of NH₃ and Faradaic efficiency at each given potential. (c) Stability tests in both N₂- and Ar-saturated electrolytes. (d) Yield of NH₃ and Faradaic efficiency under different N₂ flow rates at -0.4 V vs. RHE.

composition of the nanoparticles in the composite is Fe₃C after pyrolysis at 800 °C.³⁸ The reduced amount of metallic Fe could be attributed to the relatively high carbonization degree of the NCF composite with the additional carbon source. This indicated that iron carbide (Fe₃C) existed on NCF. It has been proven by the following electrochemical experiments that Fe₃C nanoparticles may be the active sites of NRR, which promoted the electrochemical synthesis of ammonia.

In the process of electrocatalysis, N₂ gas and Ar gas were continuously fed to the whole NCF@Ni cathode, and linear sweep voltammetry (LSV) tests were performed in Ar- and N₂-saturated 0.1 M KOH aqueous solutions at -0.4 V (vs. RHE). The LSV curves (Fig. 3a) were different in N₂ and Ar. At -0.4 V, the current density in N₂ was -2.34 mA cm⁻², which was higher than -1.85 mA cm⁻² in Ar. In a certain voltage range (from 0 to -0.5 V vs. RHE), the current density was significantly larger in nitrogen, which may be the reduction current of nitrogen, *i.e.*, NCF exhibited a significant response signal to NRR. Also, LSV performed under Ar exhibited a slightly larger current because of the catalytic current generated during HER. When the voltage was more negative than -0.5 V vs. RHE, the hydrogen evolution reaction (HER) became the main process in this catalytic system and the current density increased sharply in a short time. It is worth noting that the foam nickel electrode also has some positive effects on NRR. By measuring the absorbance curve (Fig. 3c) of a standard ammonium chloride solution, we obtained the ammonia standard calibration curve (Fig. 3d), which assisted us to obtain the yield of ammonia under different catalytic conditions. The yields of ammonia were similar for the N-doped carbon (NC@Ni)-loaded electrode, the Fe-doped carbon (CF@Ni)-loaded electrode and the non-loaded foam nickel (Ni) electrode, but the yield of ammonia for NCF was about three times that of the others (Fig. 3b). It was proved that

NCF has significant catalytic effect on electrochemical NRR and nitrogen and iron are essential. We also studied the effect of iron content on the performance of the catalyst, as shown in Fig. S6 and S8.† With an increase in the iron content, the catalytic activity increased, proving that Fe₃C is indeed the catalytic activity site. A further increase in iron content led to significant decrease in the catalyst performance, which may be caused by agglomeration of iron nanoparticles, as demonstrated by the image in Fig. S7.† The above-mentioned results proved that N and a moderate amount of iron are necessary for the catalyst.

To verify that NH₃ was produced in the NRR process, the absorption bands of the electrolyte stained with an indophenol indicator before and after electrolysis at an open potential in an N₂-saturated solution and at -0.4 V in an Ar-saturated solution are provided (Fig. 4a). No ammonia was measured at -0.4 V in the Ar-saturated solution, which could completely prove that the source of NH₃ production comes from N₂ instead of the NCF catalyst. A ¹⁵N isotopic labeling experiment was also performed to verify the N source of the produced NH₃. A triplet coupling for ¹⁴NH₄⁺ and a doublet coupling for ¹⁵NH₄⁺ in the ¹H NMR spectra were used to distinguish them. As shown in Fig. S10,† only ¹⁵NH₄⁺ was observed in the electrolyte when ¹⁵N₂ was supplied as the feeding gas, and no other reduced nitrogen species were detected; this was consistent with the results of the control experiments and confirmed that NH₃ was produced by NCF-catalyzed electroreduction of N₂. This also proved that the catalyst has excellent selectivity. In addition, we also performed relevant calculations and proved that the ammonia produced is more than the N content of the catalyst after 10 h in the electrolyte.

In order to study the effect of potential on the production rate of electrochemical synthesis of ammonia, we measured the concentration of ammonia in N₂-saturated electrolyte at different potentials. As shown in Fig. 4b and S9,† with an increase in the negative potential (from -0.2 to -0.4 V vs. RHE), the yield of ammonia and the Faraday efficiency continuously increase and reach the best values at -0.4 V vs. RHE. When the potential became more negative, the Faraday efficiency and NH₃ yield rate reduced significantly (Fig. 4b) due to the competition of the hydrogen evolution reaction, which was consistent with the sharp increase in the current density in the LSV curve. In addition to good activity, improving the stability of NRR catalysts is crucial. In order to determine the stability, chronoamperometry was performed, as shown in Fig. 4c. There was no significant decrease in the current density, which proved that the NCF catalyst has excellent stability.

The relation between NRR and gas-solid interface was verified by changing the nitrogen flow rate that led to a different contact between nitrogen and the surface of the cathode catalyst in the electrolyte. As shown in Fig. 4d, there is no significant change in the Faraday efficiency and the ammonia production rate, which proves that the relationship between the rate of electrochemical synthesis of ammonia and the gas-solid interface is negligible. Meanwhile, the rate of NRR was

independent of the concentration of N_2 in the liquid phase, indicating that the diffusion of N_2 was not a rate-determining step. The rate-determining step was still the activation of the $N\equiv N$ bond activity.

Based on the above analysis, NCF showing excellent catalytic performance may be because of the following reasons: 1) the formation of carbon nanotubes increases the specific surface area of NCF; 2) the high proportion of pyridinic N doped into NCF can promote N_2 adsorption and at the same time enhance hydrophilicity, strengthening the electrolyte-electrode interaction; 3) Fe_3C nanoparticles can be NRR active sites, which can promote the dissociation of the $N\equiv N$ bond. We could get one possible NRR process as follows: first, N_2 and H_2O approach the surface of NCF, where N_2 is fixed through carbon or pyridinic nitrogen in NCF and nearby Fe_3C nanoparticles activate it. Second, the activated H (produced by the electrolysis of H_2O) interacts with the activated nitrogen to form a more stable N-H bond and destroy the $N\equiv N$ bond. Finally, the synthesis of ammonia is carried out by adding H atoms one by one from the electrolyte.

4. Conclusions

In summary, we synthesized new non-noble metal N-doped nanocarbon/ Fe_3C nanoparticle catalysts for electrochemical synthesis of ammonia. The rate of NH_3 yield was $15.804 \mu g h^{-1} mg_{cat}^{-1}$ and the Faradic efficiency was 2.72% at $-0.4 V$ (vs. RHE) at room temperature and ambient pressure in 0.1 M KOH electrolyte. Through physical characterization and analysis, we found that pyridinic nitrogen and Fe_3C nanoparticles in NCF play important roles in NRR. We believe that this work will not only provide a new opportunity for the design of new non-noble metal catalysts for fixing nitrogen but also open up a new route to solve the global energy and ecological crises.

Conflicts of interest

There are no conflicts to declare.

Acknowledgements

This work was supported by the National Key Research and Development Program (No. 2016YFC1102802).

References

- 1 U.S. Geological Survey, *Mineral Commodity Summaries 2016*, U.S. Geological Survey, U.S. Government Publishing Office, Washington, DC, 2016, p. 118.
- 2 V. Smil, *Nature*, 1999, **400**, 415.
- 3 R. F. Service, *Science*, 2014, **345**, 610.
- 4 V. Rosca, M. Duca, M. T. De Groot and M. T. M. Koper, *Chem. Rev.*, 2009, **109**, 2209.
- 5 B. K. Burgess and D. J. Lowe, *Chem. Rev.*, 1996, **96**, 2983.
- 6 S. Licht, B. C. Cui, B. H. Wang, F. F. Li, J. Lau and S. Z. Liu, *Science*, 2014, **345**, 637.
- 7 M. A. H. J. Van Kessel, D. R. Speth, M. Albertsen, P. H. Nielsen, H. J. M. Op den Camp, B. Kartal, M. S. M. Jetten and S. Lucker, *Nature*, 2015, **528**, 555.
- 8 M. Appl, *Ammonia principles and industrial practice*, Wiley-VCH, New York, 2007.
- 9 S. A. Topham, The history of the catalytic synthesis of ammonia, in *Catalysis science and technology*, ed. J. R. Anderson and M. Boudart, Springer-Verlag, Berlin-Heidelberg, 1985, pp. 1-50.
- 10 J. M. Modak, *Resonance*, 2011, **16**, 1159.
- 11 J. A. Pool, E. Lobkovsky and P. Chirik, *Nature*, 2004, **427**, 527.
- 12 A. Varotto, *Raising the standards: Enhanced catalytic performance for global ammonia production*, 2015.
- 13 European Commission, *Large Volume Inorganic Chemicals-Ammonia, Acids and Fertilisers*, 2007.
- 14 K. Honkala, A. Hellman, I. N. Remediakis, A. Logadottir, A. Carlsson, S. Dahl, C. H. Christensen and J. K. Nørskov, *Science*, 2005, **307**, 555.
- 15 K. Kim, C. Y. Yoo, J. N. Kim, H. C. Yoon and J. I. Han, *Korean J. Chem. Eng.*, 2016, **33**, 1777.
- 16 M. M. Shi, D. Bao, B. R. Wulan, Y. H. Li, Y. F. Zhang, J. M. Yan and Q. Jiang, *Adv. Mater.*, 2017, **29**, 1606550.
- 17 T. Murakami, T. Nohira, T. Goto, Y. H. Ogata and Y. Ito, *Electrochim. Acta*, 2005, **50**, 5423.
- 18 J. M. McEnaney, A. R. Singh, J. A. Schwalbe, J. Kibsgaard, J. C. Lin, M. Cargnello, T. F. Jaramillo and J. K. Nørskov, *Energy Environ. Sci.*, 2017, **10**, 1621.
- 19 G. F. Chen, X. R. Cao, S. Q. Wu, X. Y. Zeng, L. X. Ding, M. Zhu and H. H. Wang, *J. Am. Chem. Soc.*, 2017, **139**, 9771.
- 20 X. P. Zhang, R. M. Kong, H. T. Du, L. Xia and F. L. Qu, *Chem. Commun.*, 2018, **54**, 5323.
- 21 H. T. Du, X. X. Guo, R. M. Kong and F. L. Qu, *Chem. Commun.*, 2018, **54**, 12848-12851.
- 22 I. A. Amar, C. T. Petit, L. Zhang, R. Lan, P. J. Skabara and S. Tao, *Solid State Ionics*, 2011, **201**, 94.
- 23 Y. Lu, J. Li, T. Tada, Y. Toda, S. Ueda, T. Yokoyama, M. Kitano and H. Hosono, *J. Am. Chem. Soc.*, 2016, **138**, 3970.
- 24 Y. Abghoui, A. L. Garden, J. G. Howalt, T. Vegge and E. Skulason, *ACS Catal.*, 2015, **6**, 635.
- 25 D. Bao, Q. Zhang, F.-L. Meng, H.-X. Zhong, M.-M. Shi, Y. Zhang, J.-M. Yan, Q. Jiang and X.-B. Zhang, *Adv. Mater.*, 2017, **29**, 1604799.
- 26 L. Zhang, J. Xiao, H. Wang and M. Shao, *ACS Catal.*, 2017, **7**, 7855.
- 27 Y.-H. Tian, S. Hu, X. Sheng, Y. Duan, J. Jakowski, B. G. Sumpter and J. Huang, *J. Phys. Chem. Lett.*, 2018, **9**, 570.
- 28 Y. Cao, Y. Gao, H. Zhou, X. Chen, H. Hu, S. Deng, X. Zhong, G. Zhuang and J. Wang, *Adv. Theory Simul.*, 2018, **1**, 1800018.
- 29 F. Pan, H. Zhang, K. Liu, D. Cullen, K. More, M. Wang, Z. Feng, G. Wang, G. Wu and Y. Li, *ACS Catal.*, 2018, **8**, 3116.
- 30 W. Yang, X. Liu, X. Yue, J. Jia and S. Guo, *J. Am. Chem. Soc.*, 2015, **137**, 1436.
- 31 H. Verdouw, C. Van Echteld and E. Dekkers, *Water Res.*, 1978, **12**, 399.

- 32 W. Bolleter, C. Bushman and P. W. Tidwell, *Anal. Chem.*, 1961, **33**, 592.
- 33 D. Zhu, L. Zhang, R. E. Ruther and R. J. Hamers, *Nat. Mater.*, 2013, **12**, 836.
- 34 G. Wu, N. H. Mack, W. Gao, S. Ma, R. Zhong, J. Han, J. K. Baldwin and P. Zelenay, *ACS Nano*, 2012, **6**, 9764.
- 35 S. Gupta, S. Zhao, X. X. Wang, S. Hwang, S. Karakalos, D. Su, H. Xu and G. Wu, *ACS Catal.*, 2017, **7**, 8386.
- 36 G. Wu, C. M. Johnston, N. H. Mack, K. Artyushkova, M. Ferrandon, M. Nelson, J. S. Lezama-Pacheco, S. D. Conradson, K. L. More, D. J. Myers and P. Zelenay, *J. Mater. Chem.*, 2011, **21**, 11392.
- 37 S. Mukherjee, D. A. Cullen, S. Karakalos, K. Liu, H. Zhang, S. Zhao, H. Xu, K. L. More, G. Wang and G. Wu, *Nano Energy*, 2018, **48**, 217.
- 38 X. L. Dong, Z. D. Zhang, Q. F. Xiao, X. G. Zhao, Y. C. Chuang and S. R. Jin, *J. Mater. Sci.*, 1998, **33**, 1915.